# SPACE SHUTTLE ORBITER REENTRY FLOW FIELD AND HEATING ANALYSIS

By W. C. Rochelle, TRACOR, Inc., Austin, Tex.,
B. B. Roberts, NASA/MSC, Houston, Tex.,
F. W. Vogenitz, TRW Systems, Redondo Beach, Calif.,
and L. d'Attorre, TRW Systems, Redondo Beach, Calif.

## INTRODUCTION

This paper presents the results of a study performed by TRW Systems for NASA/MSC which determined the reentry flow field and thermal environment around the straight wing Shuttle Orbiter vehicle. The objective of the study was to calculate both rarefied and continuum flow fields and associated heating rates on various configurations representative of the Orbiter at high angle of attack. Rarefied flow fields and heating rates were computed by the Monte Carlo Direct Simulation Technique for altitudes above 82.3 Km (Kn > 0.001). Continuum inviscid flow fields were calculated by 2-D unsteady and 3-D steady finite difference/artificial viscosity methods and also by a 2-D shock layer analysis technique. Viscous flow fields and heating rates in the continuum regime were computed by a boundary layer integral matrix method for laminar flow and by an aerodynamic surface heating technique for turbulent flow. Shapes considered in the study included flat plates (representing the underside of the Orbiter fuselage or the wing MAC), Orbiter fuselage cross sections, Orbiter wing airfoils, and 3-D Orbiter configurations, all at high angle of attack ($40^{o}$ - $60^{o}$). The theoretical results showed good agreement with pressure and heat transfer data obtained at NASA/MSC, NASA/Ames, NASA/Langley, and Cornell Aeronautical Laboratory (CAL).

(Figure 1)

The first figure shows a table listing all of the cases analyzed in this study by the Monte Carlo direct simulation technique for rarefied flows and by the finite difference/artificial viscosity method for continuum flows. The complete results of this study are given in Ref. 1 and a User's Manual for the Monte Carlo programs is listed as Ref. 2.

The Monte Carlo method was used for 9 cases of a flat plate at high angle of attack simulating the Orbiter wing chord. Three altitudes were considered for the flat plate: 121.8 Km, 102.2 Km, and 88.1 Km. Two cases of rarefied flow around an Orbiter cross section were considered at altitudes of 121.8 Km and 98.1 Km. In addition, a 3-D representation of the Orbiter fuselage and wings at 109.8 Km was analyzed by the Monte Carlo technique. For the cross sections and 3-D shape, a hard sphere molecular model of $\gamma = 1.67$ and $\alpha = 60^{o}$ with diffuse reflection at the surface was assumed, while for the flat plates the following parameters were varied: Knudsen No. (altitude and plate length), $\alpha$, surface reflection, molecular model, and $\gamma$.

For the finite difference analysis, 4 flat plate cases at $\alpha = 60^{o}$ were considered, two at 59.4 Km (ideal and real gas), one at 81.9 Km, and one at 88.1 Km, all of which simulated the flat underside of the Orbiter. An Orbiter cross section case at 88.1 Km at $60^{o}$ and a 3-D Orbiter configuration at 76.1 Km at $\alpha = 40^{o}$ were also analyzed with the finite difference technique. The flat plate and cross section cases were treated with a 2-D unsteady method based on a modified artificial viscosity technique to dampen out oscillations occurring across shock waves. The 3-D shape was analyzed with a 3-D steady, marching procedure along the axis of the body.

In addition to these methods, a shock layer analysis program (Ref. 3) was used to analyze the flow around 2-D Orbiter airfoils at $\alpha = 40^{o}$ and $60^{o}$ based on the finite difference input. All of the continuum heating analyses were performed with the BLIMP Program (Ref. 4) for laminar flow and either the Aerodynamic Surface Heating Program (Ref. 5) or the BLIMP C Program (Ref. 6) for turbulent flow.

# LIST OF FLAT PLATE, ORBITER CROSS SECTION, AND 3-D CASES RUN WITH FINITE DIFFERENCE AND MONTE CARLO PROGRAMS

| No. | Type | Altitude (KM) | Altitude (Kft) | Angle of Attack (°) | Mach Number | $\gamma$ | Knudsen No. ( $\lambda_\infty$ /L) | Remarks |
|---|---|---|---|---|---|---|---|---|
| | | | | **A. FLAT PLATE CASES** | | | | |
| 1 | FD | 59.4 | 195 | 60 | 13.7 | 1.4 | 6.76 E-6 | |
| 2 | FD | 59.4 | 195 | 60 | 13.7 | Var. | 6.76 E-6 | Real Gas |
| 3 | FD | 88.1 | 289 | 60 | 20 | 1.4 & Var. | .00556 | Compare with CAL Data |
| 4 | FD | 81.9 | 269 | 60 | 28.3 | 1.4 | .00139 | |
| 5 | MC | 121.8 | 400 | 60 | 28.5 | 1.67 | .994 | |
| 6 | MC | 102.2 | 335 | 60 | 28.5 | 1.67 | .0556 | |
| 6a | MC | 102.2 | 335 | 60 | 28.5 | 1.4 | .0556 | |
| 7 | MC | 102.2 | 335 | 45 | 28.5 | 1.67 | .0556 | |
| 8 | MC | 88.1 | 289 | 60 | 20 | 1.67 | .00556 | Compare with CAL Data |
| 8a | MC | 88.1 | 289 | 60 | 20 | 1.4 | .0111 | |
| 9 | MC | 102.2 | 335 | 60 | 28.5 | 1.67 | .0556 | 30% Specular Reflection |
| 10 | MC | 102.2 | 335 | 60 | 28.5 | 1.67 | .0556 | 12th Power Molecular Model |
| 11 | MC | 88.1 | 289 | 60 | 20 | 1.4 | .00556 | Compare with CAL Data |
| | | | | **B. ORBITER CROSS SECTION CASES** | | | | |
| 1 | FD | 81.9 | 269 | 60 | 28.3 | 1.4 | .001 | Kn = $\lambda_\infty$ / D |
| 2 | MC | 121.8 | 400 | 60 | 28.5 | 1.67 | .721 | Kn = $\lambda_\infty$ / D |
| 3 | MC | 98.1 | 322 | 60 | 24.0 | 1.67 | .02 | Kn = $\lambda_\infty$ / D |
| | | | | **C. 3-D CASES** | | | | |
| 1 | FD | 76.1 | 250 | 40 | 26.65 | 1.4 | 6.41 E-5 | 26.5° Half Angle Cone for Nose |
| 2 | MC | 109.8 | 360 | 60 | 28.5 | 1.67 | .0117 | Channel Section with Cyl. Top |

**NOTE:** All M.C. calculations performed with hard sphere molecular model with diffuse reflection at walls except as noted.

Figure 1

(Figure 2)

Figure 2 shows the cell structure for flow over a flat plate at 102.2 Km for computation by the Monte Carlo method. Notice that there are three types of layers of cells with the smallest layers near the body where the changes in flow properties are the greatest. In a particular cell, pairs of molecules are selected at random and are retained for collision with probability proportional to their relative velocity raised to an exponent whose value depends upon the molecular model (hard sphere, Maxwell, 1/12 power, energy sink, etc.).

In the total flow field a relatively small number of molecules (of the order of several thousand) compared to the number in an actual gas is set in uniform motion in a field of size sufficient to contain the disturbance caused by the body. The molecules are distributed uniformly in space, and their velocity components are assigned by sampling from a distribution which is Maxwellian about the free stream velocity. The molecular paths between collisions are computed exactly but collisions are treated statistically. The calculation procedure consists of holding all molecules motionless for a time interval while collisions are computed in the field, and then allowing the molecules to move with their new velocities for another time interval. After a time interval has passed sufficient for the mean flow to traverse a distance of a few body lengths the flow is considered to be sufficiently close to the steady state. In this manner a collection of simulated molecules numbering many orders of magnitude less than those in the real gas behaves on the average as does the collection of real molecules, and by continuing the calculation for a sufficiently long time an accurate description of the flow field and surface properties can be obtained.

## CELL ARRANGEMENT FOR FLOW OVER FLAT PLATE AT ANGLE OF ATTACK AT 102.2 KM

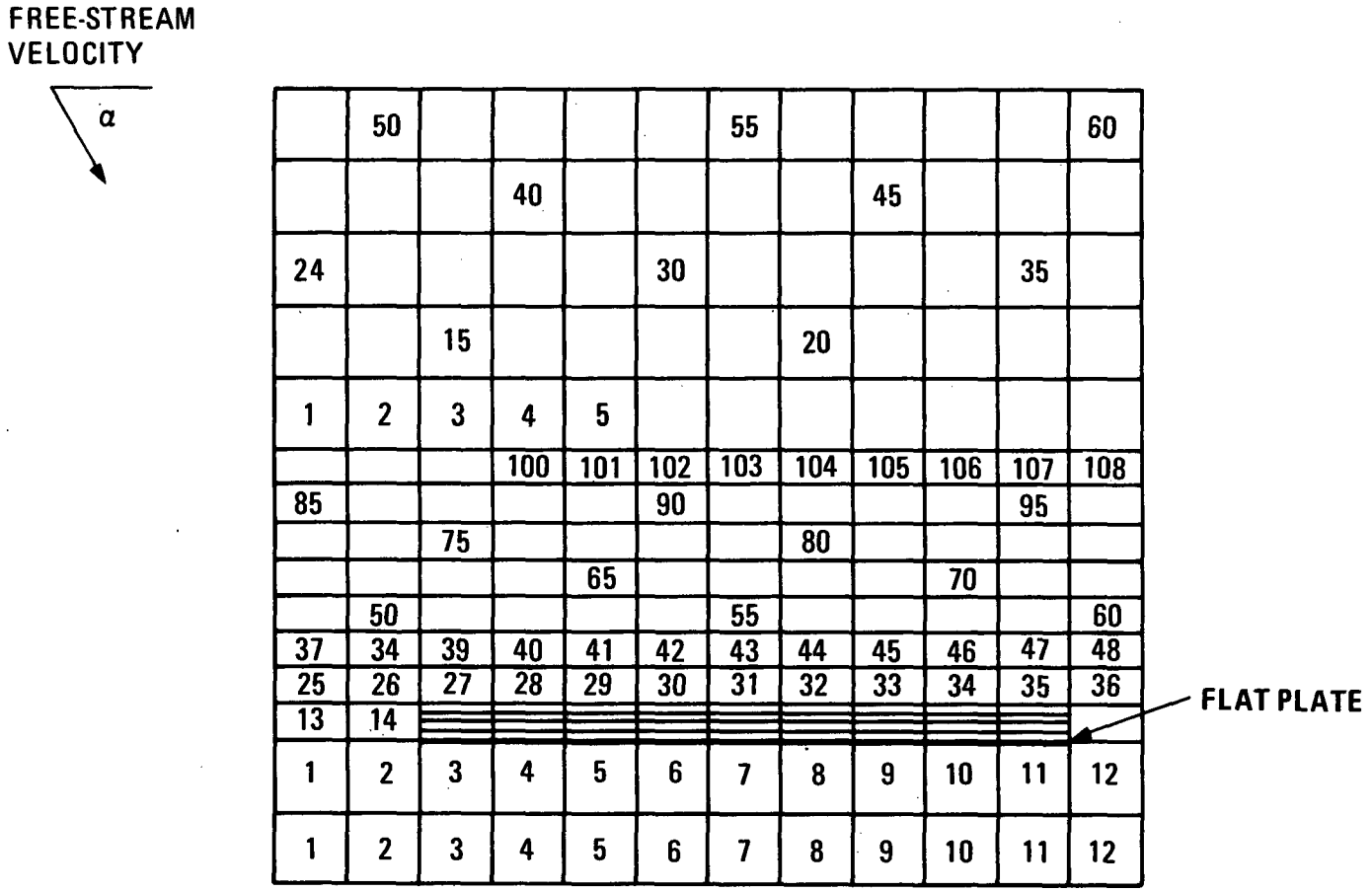


| | | | | | | | | | | | |
|---|---|---|---|---|---|---|---|---|---|---|---|
| | 50 | | | | | 55 | | | | | 60 |
| | | | 40 | | | | | 45 | | | |
| 24 | | | | | 30 | | | | | 35 | |
| | | 15 | | | | | 20 | | | | |
| 1 | 2 | 3 | 4 | 5 | | | | | | | |
| | | | 100 | 101 | 102 | 103 | 104 | 105 | 106 | 107 | 108 |
| 85 | | | | | 90 | | | | | 95 | |
| | | 75 | | | | | 80 | | | | |
| | | | | 65 | | | | | 70 | | |
| | 50 | | | | | 55 | | | | | 60 |
| 37 | 34 | 39 | 40 | 41 | 42 | 43 | 44 | 45 | 46 | 47 | 48 |
| 25 | 26 | 27 | 28 | 29 | 30 | 31 | 32 | 33 | 34 | 35 | 36 |
| 13 | 14 | | | | | | | | | | |
| 1 | 2 | 3 | 4 | 5 | 6 | 7 | 8 | 9 | 10 | 11 | 12 |
| 1 | 2 | 3 | 4 | 5 | 6 | 7 | 8 | 9 | 10 | 11 | 12 |

Figure 2

(Figure 3)

This figure shows the results of 5 Monte Carlo calculations of heating rate to a flat plate at 102.2 Km for Kn = 0.0556 which corresponds to an Orbiter wing chord of 4.24 meters. Four parameters have been varied: angle of attack, type of surface reflection at the wall, molecular model, and ratio of specific heats. In all cases the heating rate increases as the leading edge is approached but remains below the free molecular value for each case. The heating rates are lowest for the $\alpha = 45^{o}$ case since the free molecular heat transfer coefficient is proportional to the cosine of the angle between the freestream velocity vector and the surface normal. Also, when the wall is 30% specularly reflective, the heat transfer is reduced since the free molecular heat transfer coefficient is proportional to the accomodation coefficient which is 0.7 for this case. The heating rate coefficient is highest for the diatomic hard sphere gas which has an extra component of rotational heat transfer due to the internal energy of the impinging molecules. For the case of the 1/12 power molecules the heating rates are essentially the same as the case of hard spheres for the same $\alpha$, $\gamma$, and surface reflection.

## EFFECTS OF $\alpha$, MOLECULAR MODEL, $\gamma$, AND SURFACE REFLECTION ON HEAT TRANSFER TO FLAT PLATE AT 102.2 M (335 KFT) USING MONTE CARLO METHOD

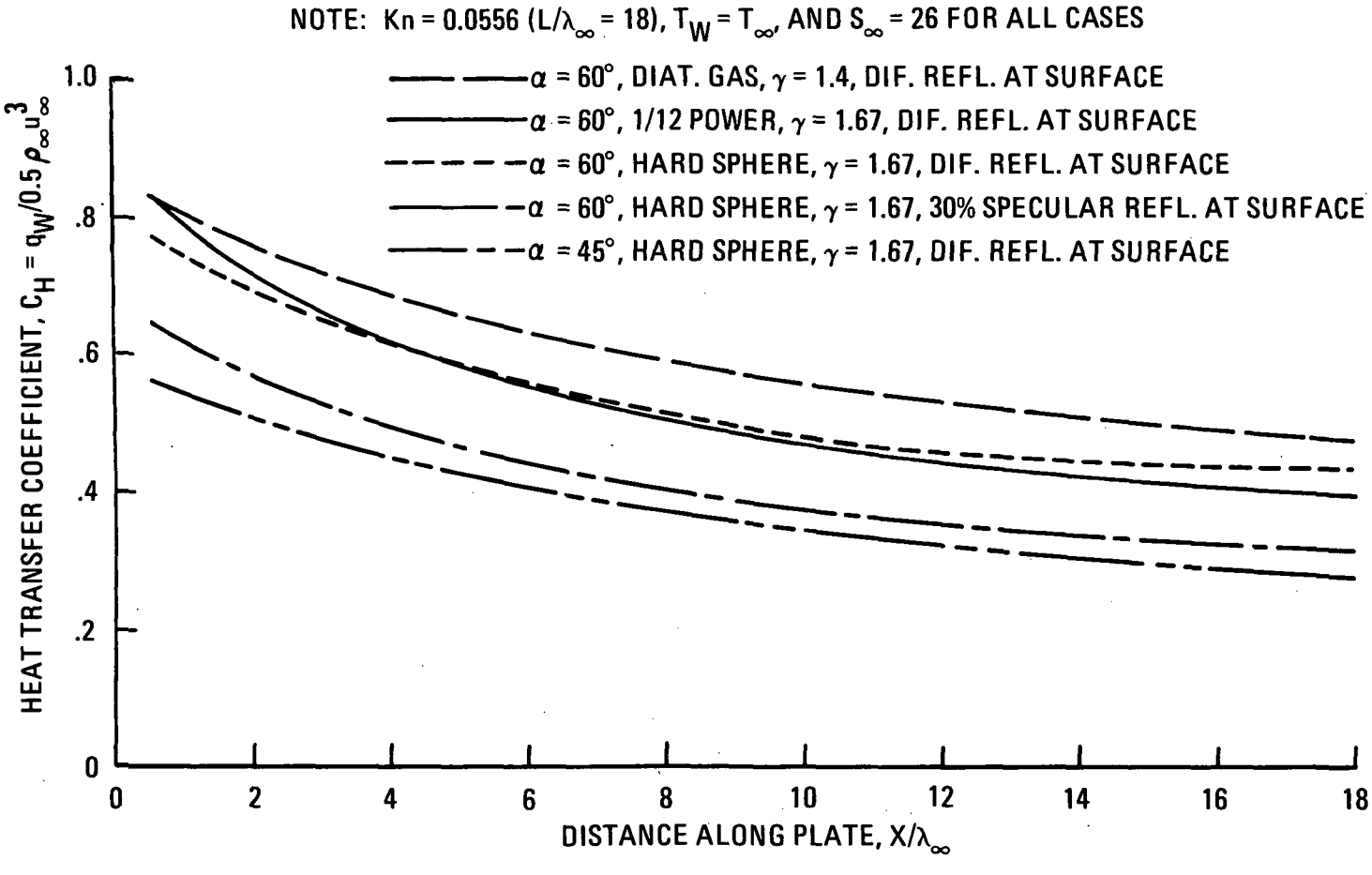


Figure 3

(Figure 4)

In this figure the cell structure around an Orbiter cross section at 121.8 Km is shown as computed by the Monte Carlo Method. For this case the Knudsen No. = $\lambda_w/D = 0.721$ with an angle of attack of $60^o$. A monatomic ($\gamma = 1.67$) hard sphere gas was assumed with diffuse reflection at the walls. The large number of small cells are needed in the stagnation region where the density rapidly rises. At this altitude, however, the shock layer was found to be fully merged with no distinct shock wave or boundary layer.

## MONTE CARLO CELL CONFIGURATION FOR ORBITER CROSS-SECTION AT ANGLE OF ATTACK AT 121.8 KM, KNUDSEN NUMBER = $\lambda_\infty/D = 0.721$

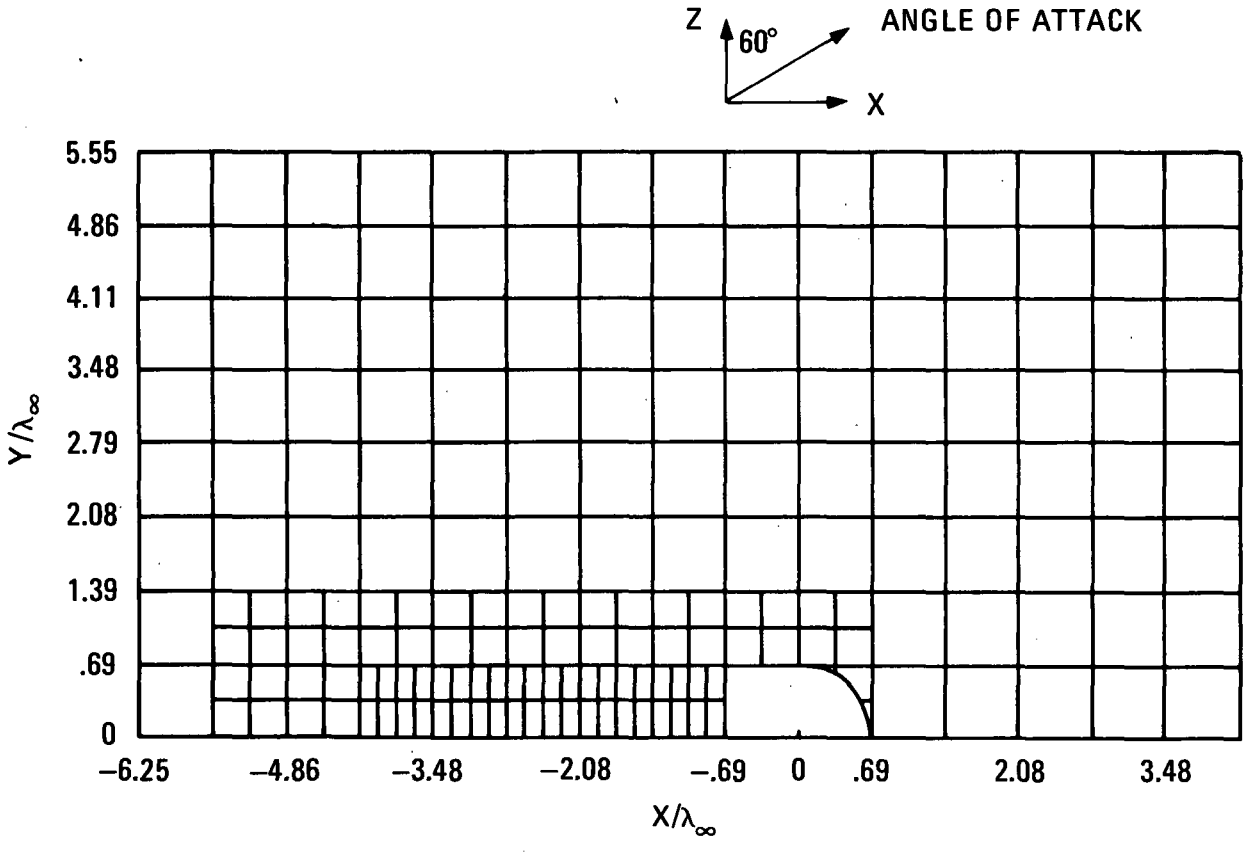


Figure 4

(Figure 5)

The local heat transfer coefficient computed by the Monte Carlo method for the Orbiter cross section is shown in the next figure as a function of the distance measured along the surface from the stagnation line. At an altitude of 121.8 Km the average heat transfer coefficient is about 0.54 while the free molecular value is about 0.87. On the flat side the average heat transfer coefficient is about 0.094 while the value calculated from free-molecular theory is 0.011. At an altitude of 98.1 Km at $\alpha = 60^{o}$, the average heat transfer coefficient on the front face is about 0.3 while on the flat side the average value is about 0.05. It is thus seen that heating rates to the flat side are under predicted by free-molecule theory by a factor of about 4 or 5 at 98.1 Km and by a factor of about 9 at 121.8 Km.

## LOCAL SURFACE HEAT TRANSFER DISTRIBUTION ON THE ORBITER CROSS-SECTION AT 60° ANGLE OF ATTACK AT 121.8 KM AND 102.2 KM USING MONTE CARLO METHOD

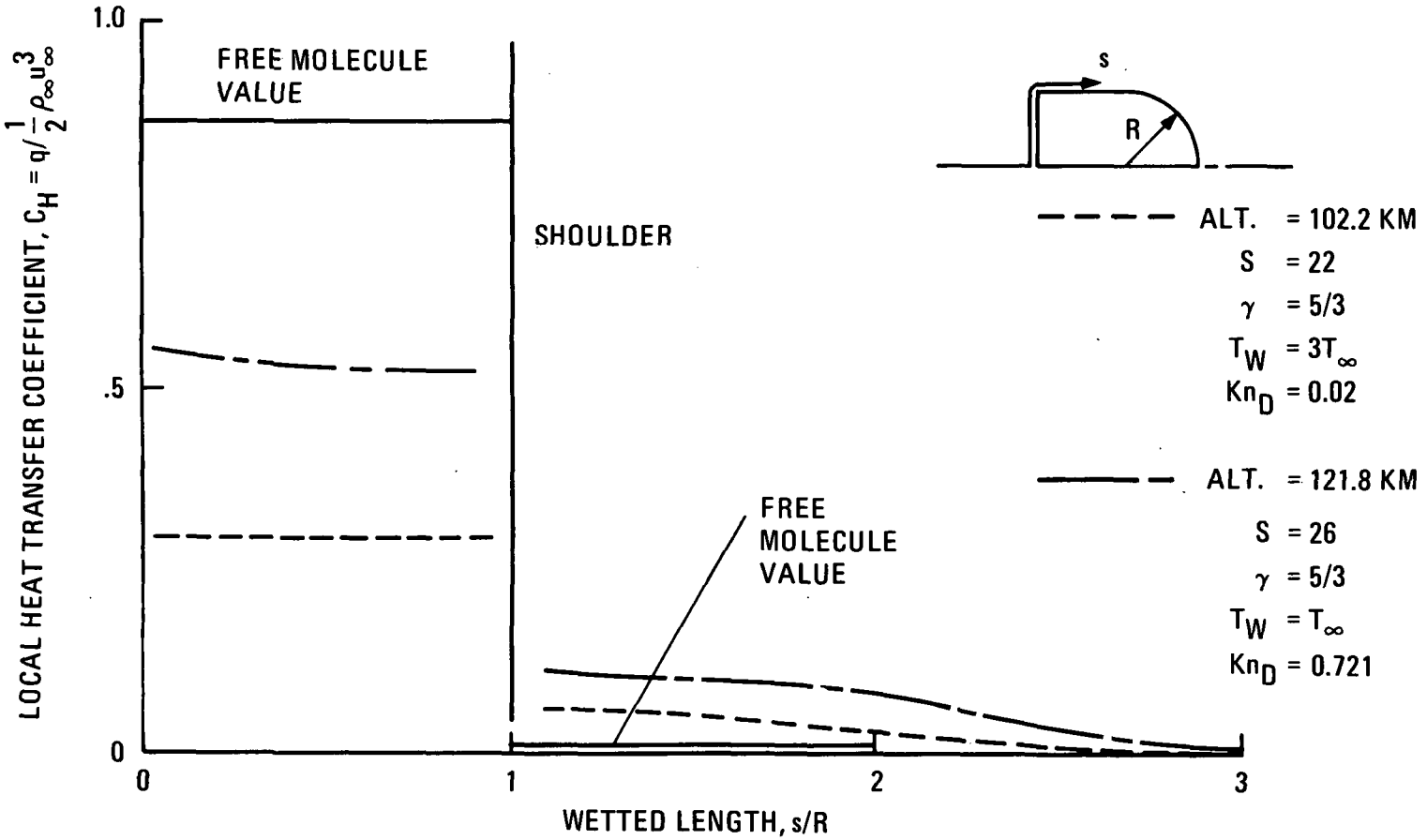


Figure 5

(Figure 6)

The next figure shows a comparison between Monte Carlo and finite difference calculations of pressure coefficient on a flat plate at $\alpha = 60^{o}$ corresponding to the test conditions of Vidal and Bartz at CAL (Ref. 7). The pressure data were taken on a flat plate of length $L = 180\lambda_{\infty}$ with the measurements made on the first half of the plate. This data was selected for comparison because at the time this was the only existing flat plate data (as determined by the survey of Ref. 8) at high enough angle of attack to be considered representative of Orbiter reentry conditions.

Monte Carlo calculations were made for a diatomic gas ($\gamma = 1.4$) for a plate length of $L = 90\lambda_{\infty}$ and finite difference calculations were made for $L = 180\lambda_{\infty}$. The fact that the Monte Carlo pressures were somewhat lower than the data is presumably due to the difference in plate length since at $60^{o}$ angle of attack the "trailing edge effect" would be expected to be significantly large over much of the plate. The finite difference calculations were made for an ideal gas ($\gamma = 1.4$) and for a real gas of variable $\gamma$. It is seen that the real gas curve was higher at the stagnation region and oscillated somewhat while the ideal gas distribution was relatively flat in the stagnation region.

**PRESSURE COEFFICIENT COMPARISON ON FLAT PLATE AT 60° ANGLE OF ATTACK WITH EXPERIMENTAL DATA OF VIDAL AND BARTZ**

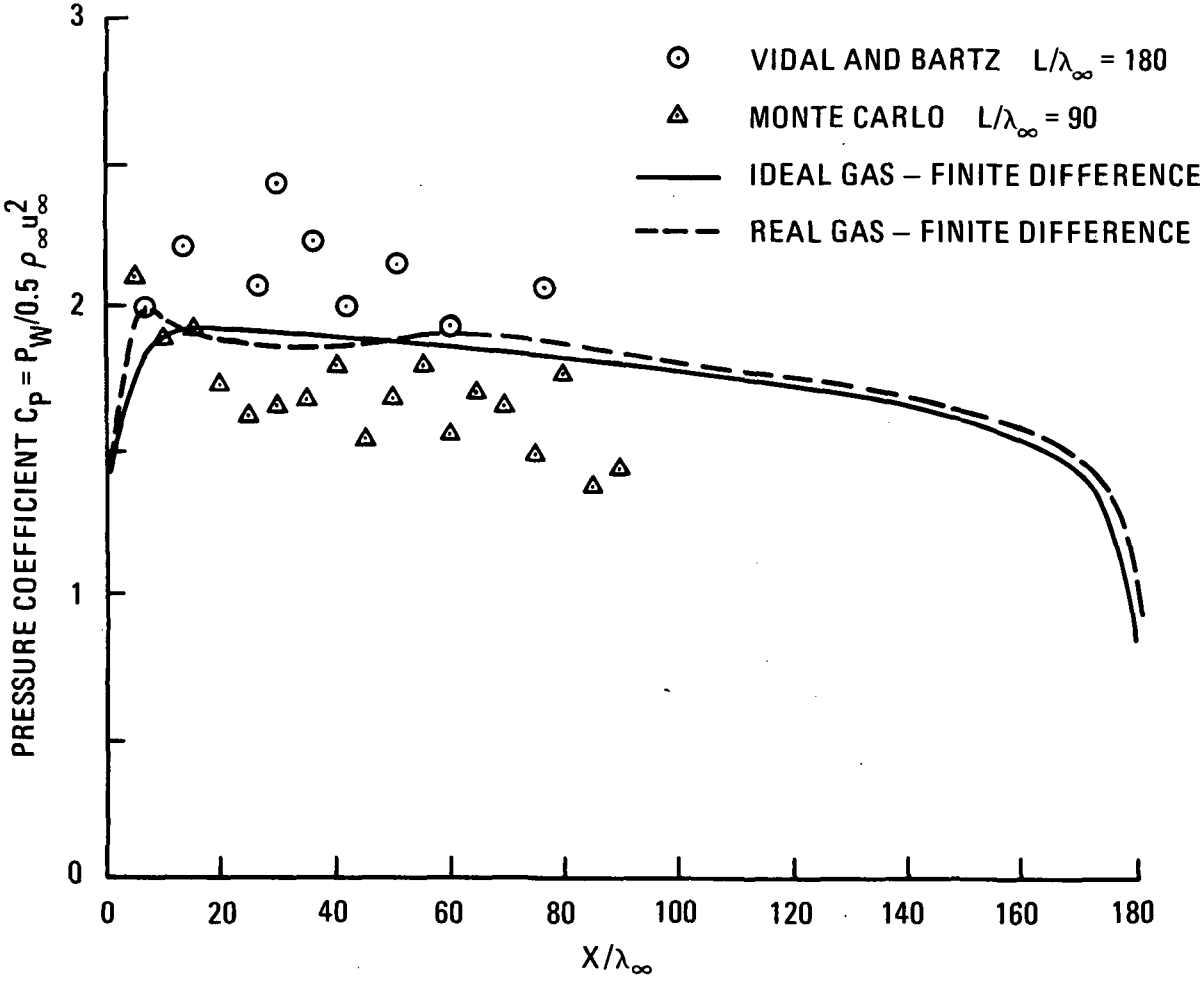


Figure 6

(Figure 7)

This figure shows the heat transfer coefficients computed by the Monte Carlo method for plate lengths of $L = 18\lambda_\infty$ and $90\lambda_\infty$ compared with the CAL data (Ref. 7) for plate lengths of $L = 18\lambda_\infty$ and $180\lambda_\infty$. Also shown are the BLIMP laminar heating rate calculations based on the finite difference ideal and real gas flow fields.

The Monte Carlo results for the shorter plate are in excellent agreement with the experimental data over the entire instrumented plate length. The Monte Carlo calculations for the plate length $L = 90\lambda_\infty$ agree well with the data for about the first 30 mean free paths, but depart from the data on the downstream portion. Again, the most likely source of this difference is a "trailing edge effect" due to the plate length.

The finite difference/BLIMP heating results showed better agreement with the CAL heating rate data near the leading edge using the real gas analysis but better agreement near the trailing edge using the ideal gas analysis. The reason for this can be partly explained by viewing the next figure.

## HEAT TRANSFER COMPARISON ON FLAT PLATE AT 60° ANGLE OF ATTACK WITH EXPERIMENTAL DATA OF VIDAL AND BARTZ

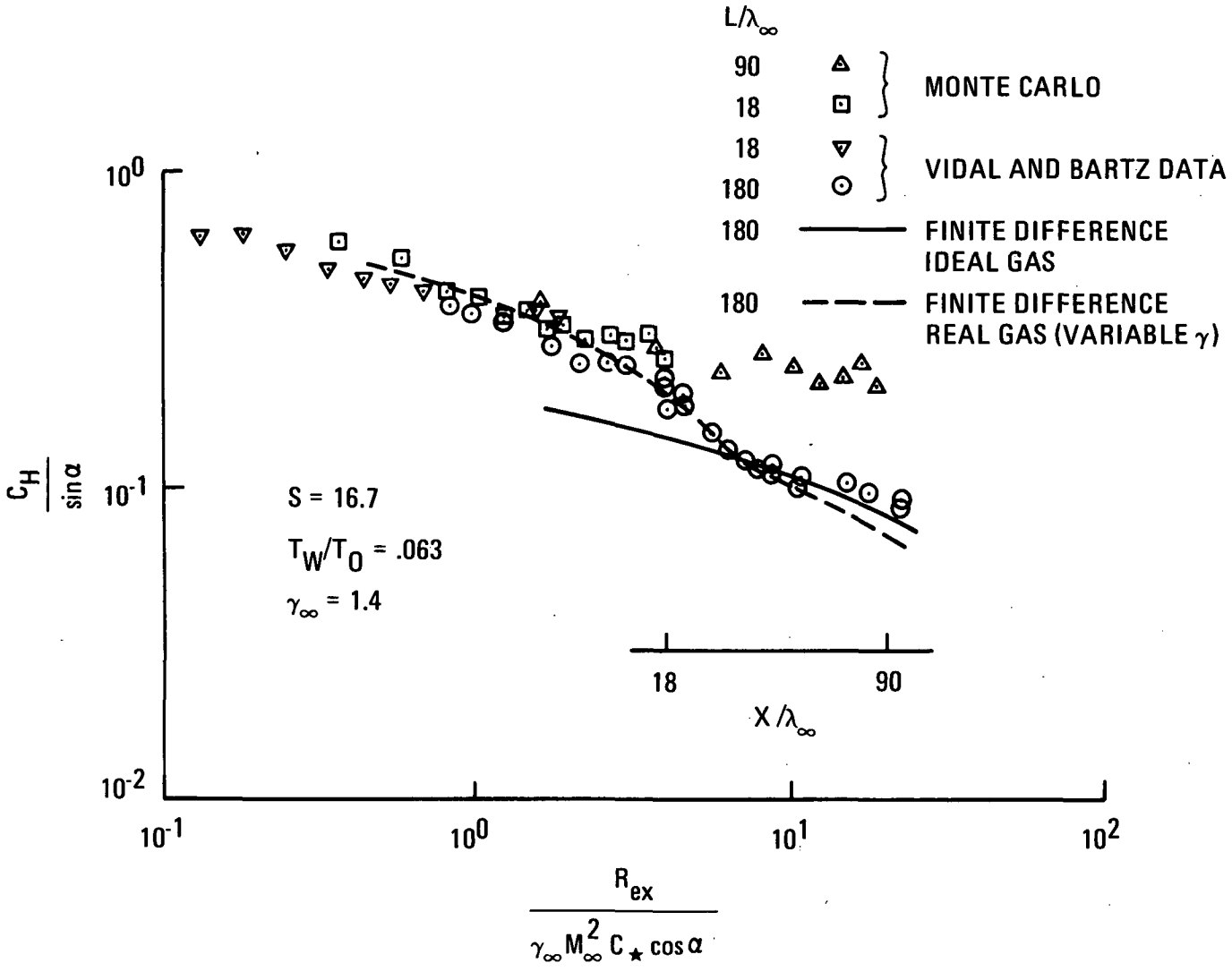


Figure 7

(Figure 8)

This figure shows the sonic lines and shock waves for this flat plate of Vidal and Bartz as computed by both the ideal and real gas finite difference analyses. For the real gas case the stagnation point lies closer to the leading edge than for the ideal gas, resulting in steeper pressure and velocity gradients (and hence higher heating rates in this region). Note that the sonic line and shock wave are closer to the plate for the real gas than for the ideal gas analysis.

FLOW-FIELD MESH, SONIC LINE AND SHOCK WAVE FOR ORBITER CROSS SECTION AT 60° ANGLE OF ATTACK, $V_\infty$ = 7.84 KM/SEC, COMPUTED BY 2-D UNSTEADY FINITE DIFFERENCE METHOD

NOTE: EACH UNIT OF M AND N = 0.00763 METERS (0.025 FT)

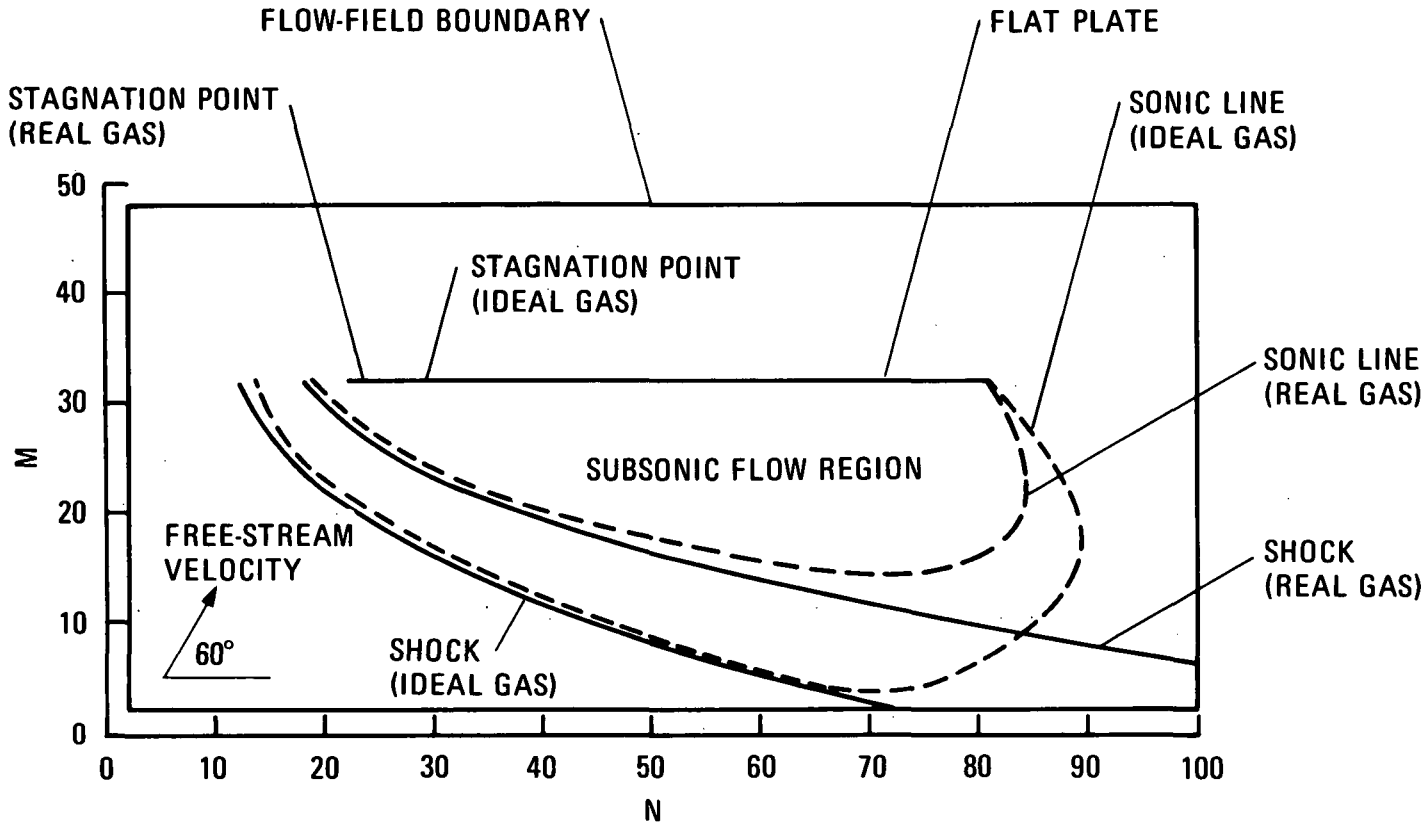


Figure 8

(Figure 9)

In this figure the Mach No. distribution along a flat plate at $60^{o}$ angle of attack as calculated by the finite difference method is shown. For this particular case the altitude was 59.4 Km, the velocity was 4.45 Km/sec, and the plate length was taken to be 36.6 meters, corresponding to the length of the flat underside of the Orbiter fuselage. Note the large region of subsonic flow along nearly the entire length of the plate (and consequently the Orbiter fuselage).

## MACH NO. DISTRIBUTION ALONG FLAT PLATE (M = 32) AT 60° ANGLE OF ATTACK FOR CYCLE 800

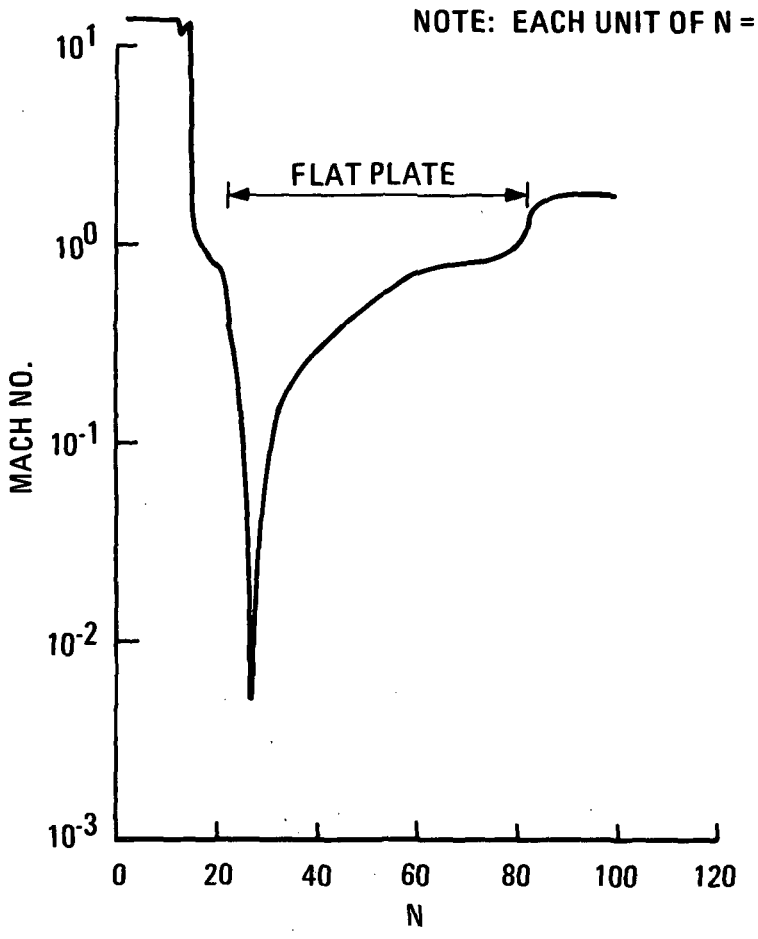


Figure 9

(Figure 10)

Heating rates along the same flat plate discussed in the previous figure are shown in this figure. Also shown for comparison is the fairing of the Orbiter fuselage heating data taken from Langley paint tests (Ref. 9). Reasonably good correlation with the heating rate data occurred when the 2-D laminar heating rates were corrected for 3-D effects. The curve marked turbulent in the figure occurs for the actual 36.6 meter plate at these conditions; however, the flow field for the Langley tests was purely laminar ($Re < 10^5$) along the fuselage so that the data did not exhibit a rise in heating due to turbulent flow.

## COMPARISON OF HEATING RATES ALONG FLAT PLATE AT 60° ANGLE OF ATTACK WITH NASA/LANGLEY ORBITER PAINT TEST DATA

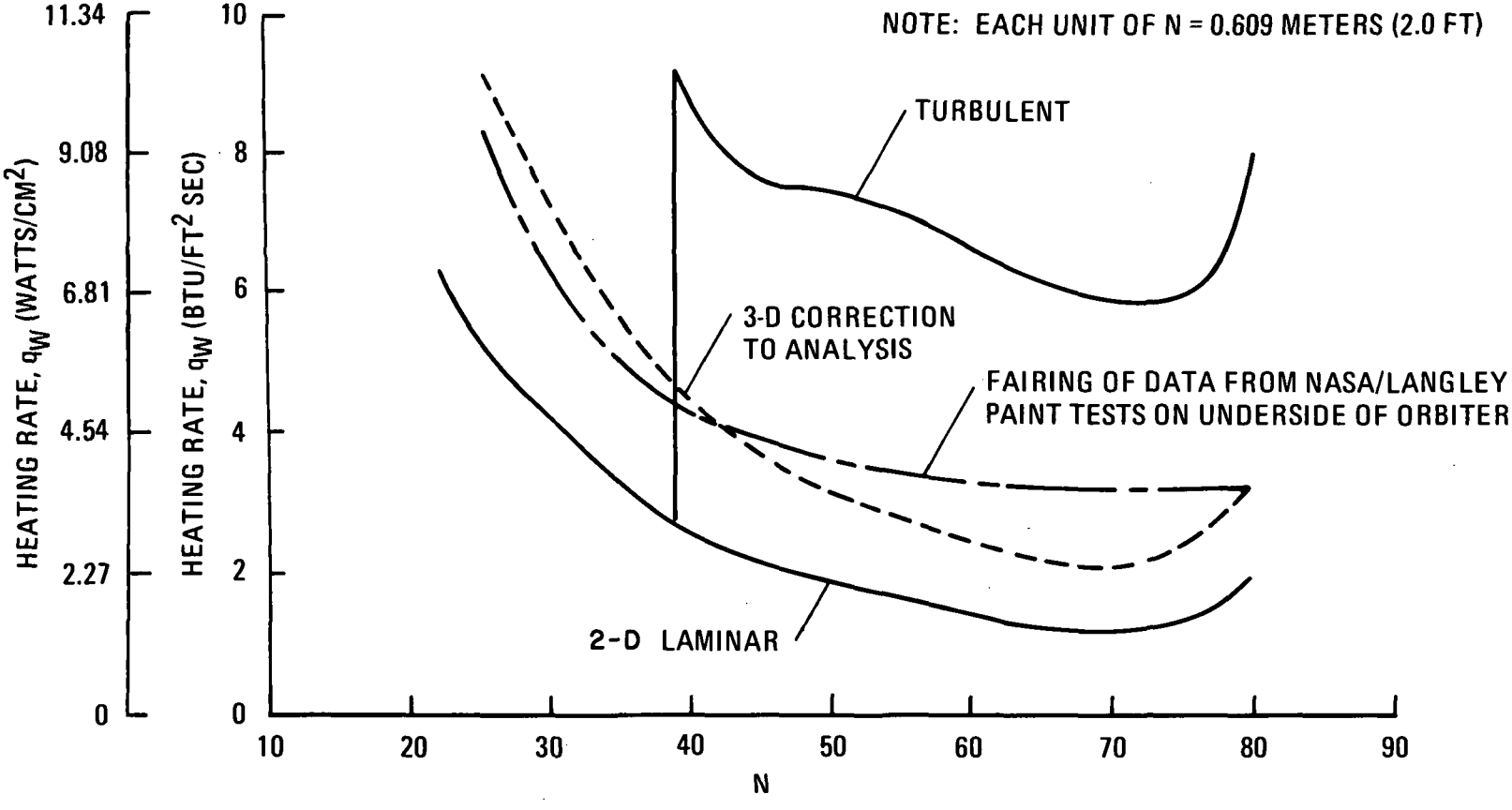


Figure 10

(Figure 11)

The finite difference 2-D unsteady technique was used to predict the flow field and shock structure around an Orbiter cross section as seen in figure 11. This case was for 81.9 Km altitude and free stream Mach No. of 28.3. The shock waves and sonic lines shown are based on ideal gas flow and the calculations were stopped at cycle 980 which was effectively steady state. Notice the large subsonic region in the neighborhood of the stagnation point. There is also a subsonic flow region at the top of the cross section which for the actual Orbiter will be all separated flow. The pressure distribution varied by some three orders of magnitude around this cross section and the heating rates by some two orders of magnitude, as will be seen in a later figure. The results of this analysis were used as input to an analysis of an airfoil at $60^{o}$ angle of attack and also served to provide basic flow field knowledge for the 3-D finite difference calculations discussed in the next figure.

**FLOW-FIELD MESH, SONIC LINE AND SHOCK WAVE FOR FLAT PLATE AT 60° ANGLE OF ATTACK, V = 3.14 KM/SEC, COMPUTED BY 2-D UNSTEADY FINITE DIFFERENCE METHOD**

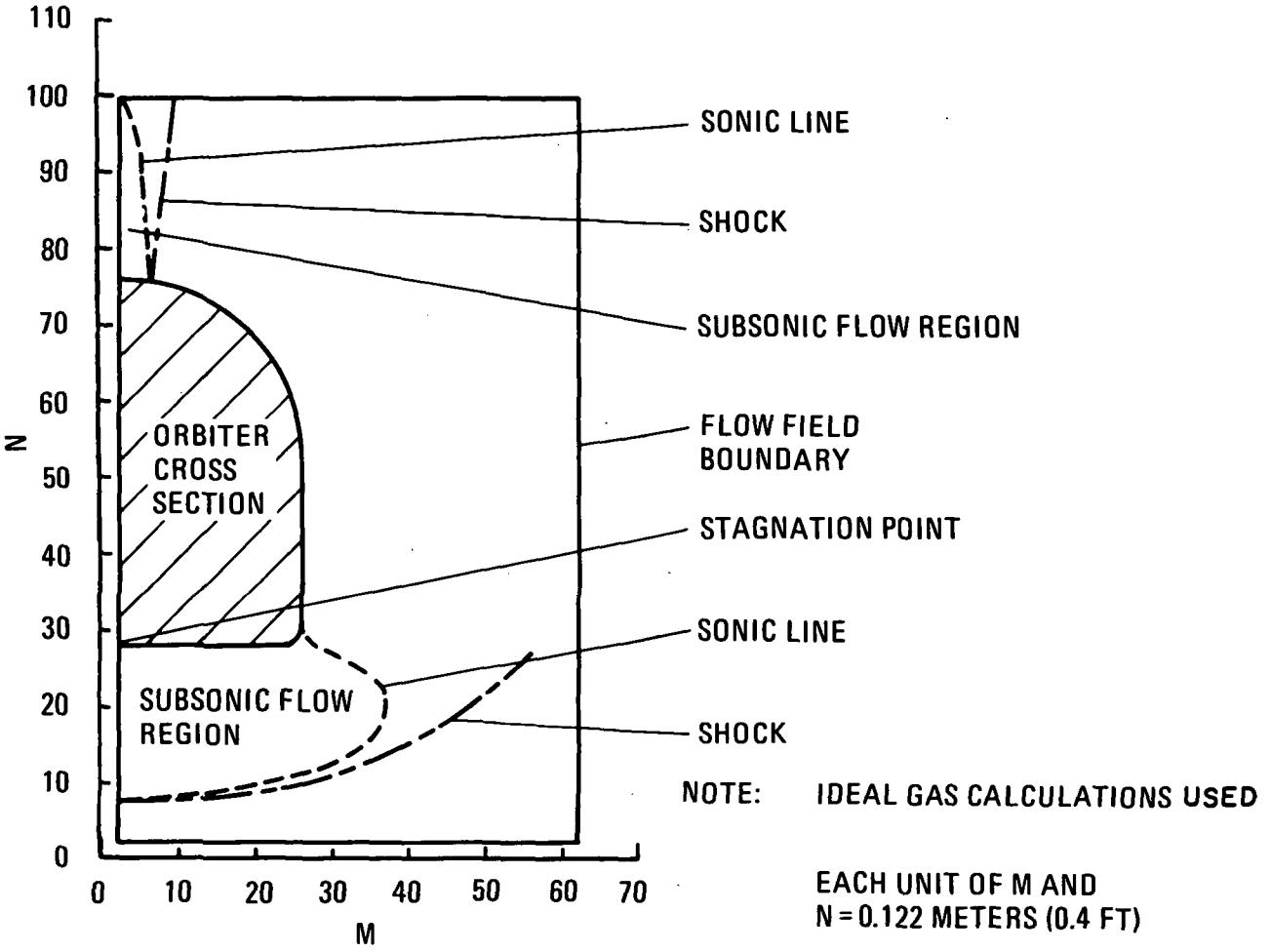


Figure 11

(Figure 12)

This figure shows a 3-D representation of the Orbiter fuselage and wings as analyzed by the 3-D steady finite difference method at an altitude of 76.1 Km. This method was used to calculate the flow field around the 3-D body at an angle of attack which was low enough (i.e., $40^{o}$) to maintain supersonic flow all along the body. The nose of the body was pointed such that the shock remained attached to the body and the flow was completely supersonic as compared to the subsonic/supersonic 2-D unsteady flow fields discussed previously.

The 3-D method of analysis was based on the numerical solution of the finite difference analog of the hyperbolic equations that represented the inviscid flow. The numerical scheme of computation was an explicit one where a marching procedure along one of the three space coordinates was used. The flow calculation progresses from an initial surface to the next parallel surface whereupon the flow is calculated and the new flow values are used for computation of the next surface. The procedure is repeated until the entire range of interest is covered, which was for our case about the midpoint of the Orbiter wing or about 1200 cycles beyond a cone calculation of about 200 cycles. The most accurate cone that approximated the front part of the fuselage was a $26.5^{o}$ half-angle cone with its axis at an angle of $11.5^{o}$ to the main axis of the fuselage. This conical surface was gradually tapered into the fuselage cross section some distance downstream of the nose as seen in the next figure.

## 3-D ORBITER FUSELAGE CONTOUR USED IN 3-D STEADY FINITE DIFFERENCE CALCULATIONS

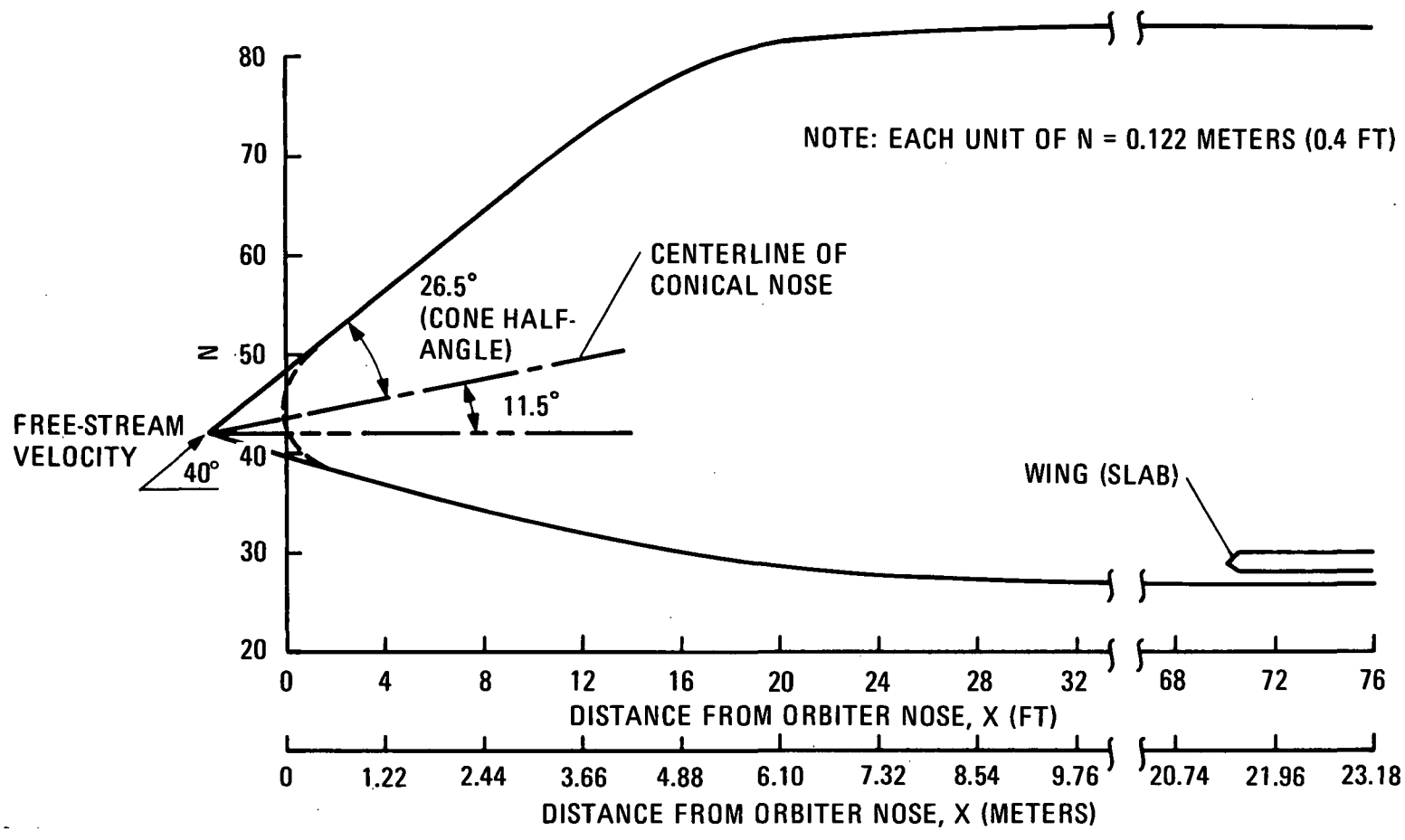


Figure 12

(Figure 13)

Some of the 3-D Orbiter fuselage cross sections and shock waves are shown in this figure. The fuselage bow shocks become increasingly larger until the fuselage changes into its constant contour between cycle 680 and 1020 during which time the shocks do not increase significantly. At roughly cycle 1010 or about 21.6 meters from the nose the wing was reached. The peak in pressure along the span moves outward until it is at about 37% of the span of the wing at about 1 meter back on the chord.

## 3-D ORBITER FUSELAGE CROSS SECTIONS AND SHOCKS COMPUTED BY FINITE DIFFERENCE METHOD

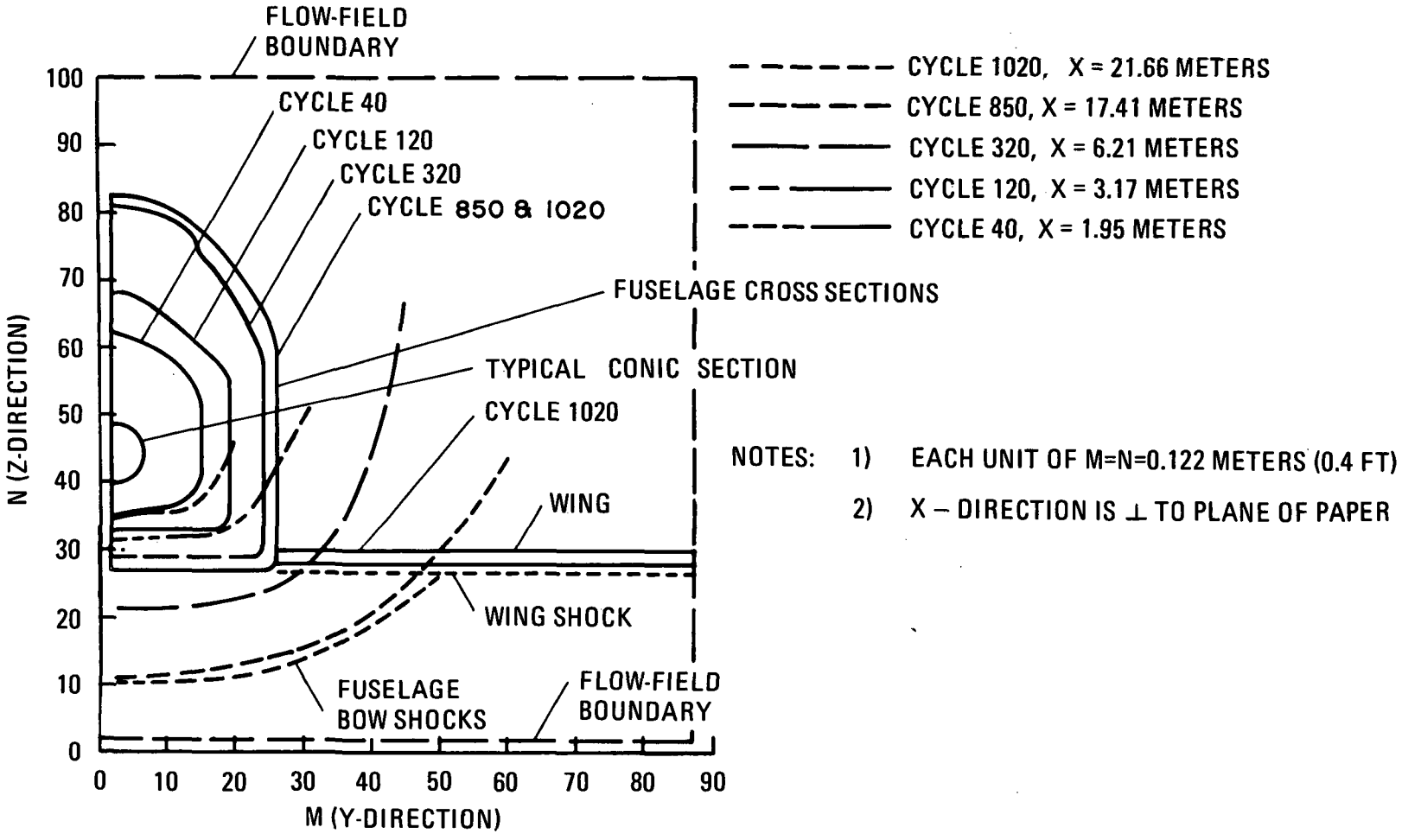


Figure 13

(Figure 14)

The calculated finite difference pressures on the bottom of the fuselage for $\alpha = 40^{o}$ are shown compared with recent NASA/Ames test data ( C. Pappas) for a North American Rockwell straight wing Orbiter configuration. The finite difference calculations show remarkedly good correlation with the test data for $\alpha = 45^{o}$. These pressures were used to compute heating rates along the bottom of the fuselage as seen in the next figure.

## PRESSURES ON UNDERSIDE OF ORBITER FUSELAGE AT VARIOUS ANGLES OF ATTACK

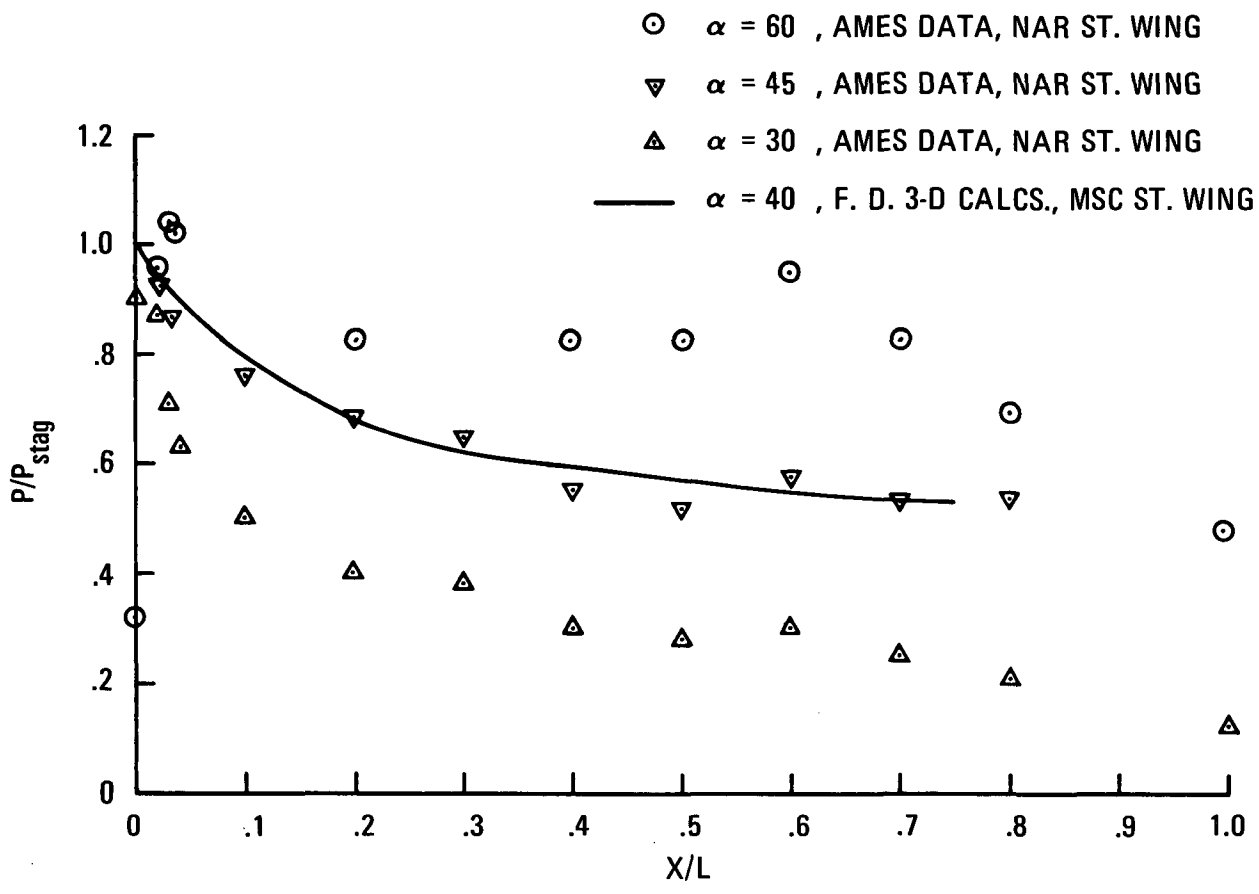


Figure 14

(Figure 15)

Heating rates along the underside of the Orbiter fuselage at $\alpha = 40^{\circ}$ as predicted by the BLIMP laminar and turbulent programs are shown in this figure. These calculations which are based on the previous pressure distributions are compared with Ames test data of Ref. 10 for the MSC straight wing Orbiter. Note the very good correlation for laminar flow using the 3-D axisymmetric option of BLIMP. The turbulent curve shown resulted only when the Ames test conditions were used since for the actual vehicle at this point in a $40^{\circ}$ trajectory the transition point would not occur until a value of X/L of about 0.8 was reached.

## HEATING RATES ON UNDERSIDE OF ORBITER FUSELAGE AT 40° ANGLE OF ATTACK

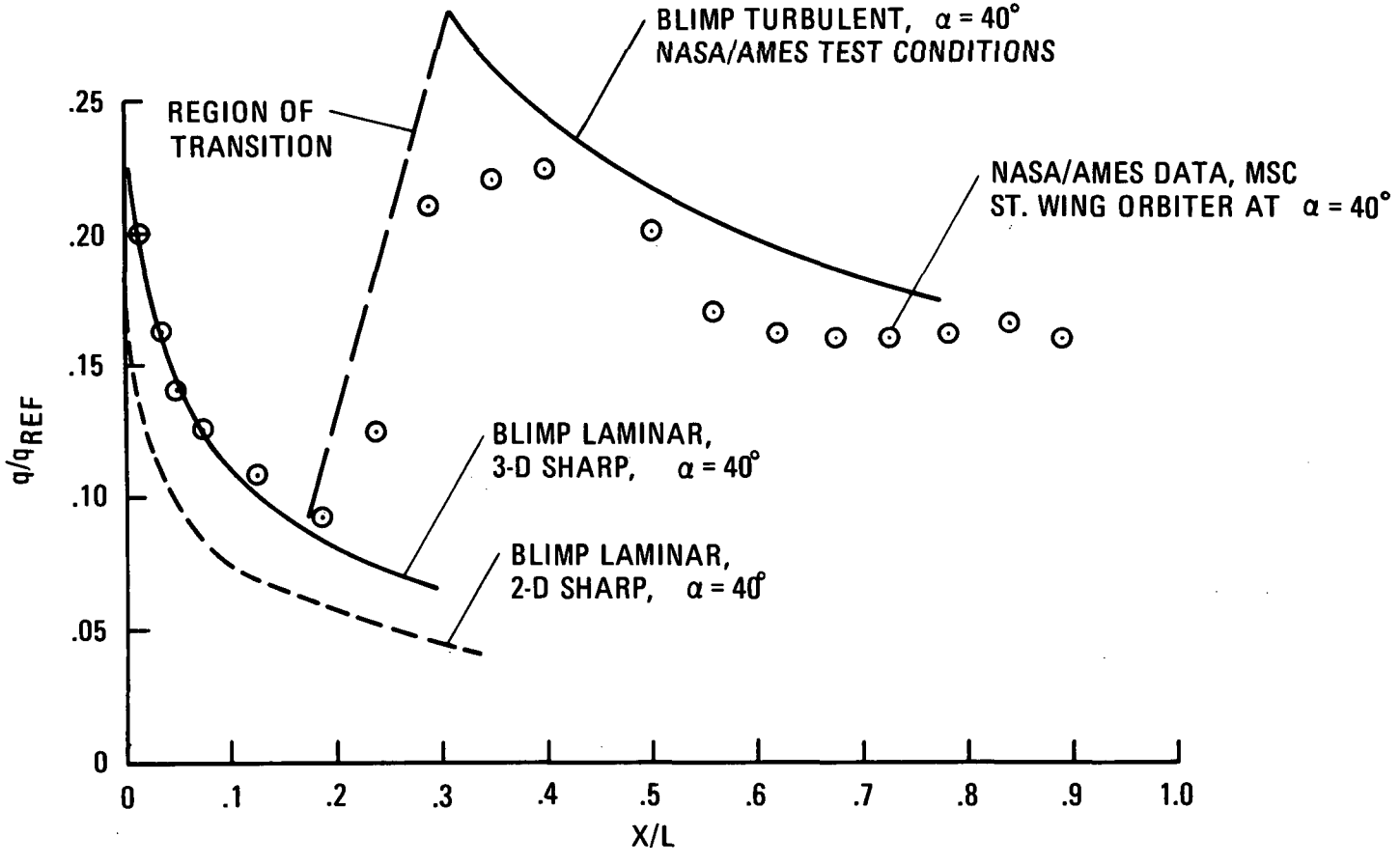


Figure 15

(Figure 16)

Surface pressures predicted by the 3-D steady finite difference program along a cross section at X/L of 0.2 are shown in this figure. Good correlation is seen between the 3-D calculations and Ames test data for the NAR straight wing Orbiter obtained from Ref.10 at this station (and also at several other stations not shown). Pressure distribution calculations at stations such as these were used to input to heating calculations such as seen in the next figure.

**PRESSURES ON CROSS SECTION OF ORBITER FUSELAGE AT X/L = 0.2**
**COMPUTED BY FINITE DIFFERENCE METHOD**

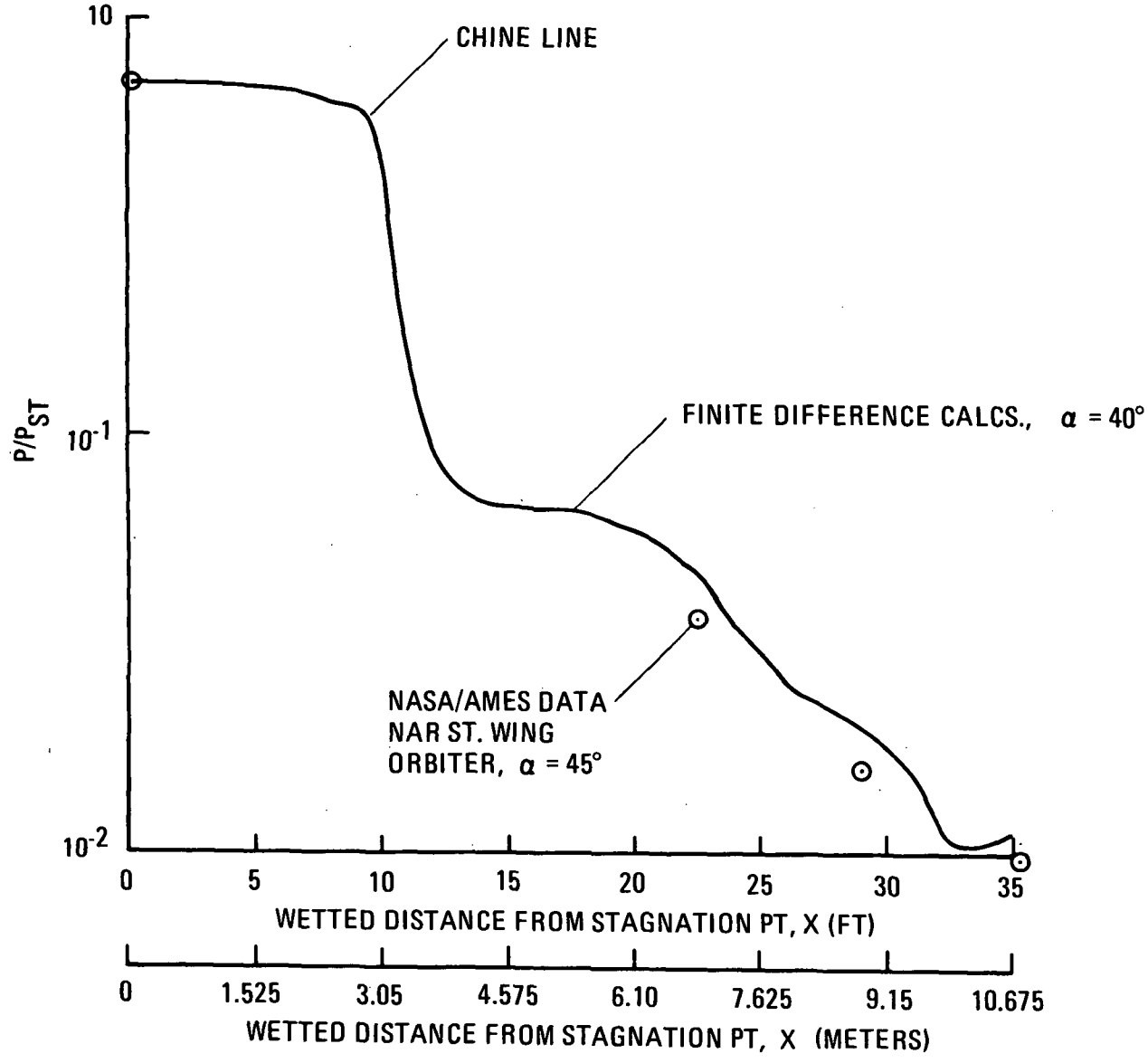


Figure 16

(Figure 17)

This figure shows calculations made along a cross section at X/L = 0.45 based on the 3-D steady finite difference pressures for $\alpha = 40^{o}$. Since no heating rate data on the side of the Orbiter fuselage could be found for $\alpha = 40^{o}$ a data point for an MSC Arc-Jet Test (by C. Scott) for $\alpha = 60^{o}$ was used. The heating rate calculation shown for $\alpha = 40^{o}$ represents fairly good correlation with the data as the data is somewhat higher for $\alpha = 60^{o}$. Notice the large increase in heating rate at the chine line (a factor of nearly 2) even though there is a drop in pressure at the chine line. This is due to the rapid acceleration of the flow toward the corner and was observed in the MSC tests.

## HEATING RATES ON CROSS SECTION OF ORBITER FUSELAGE AT X/L = 0.45

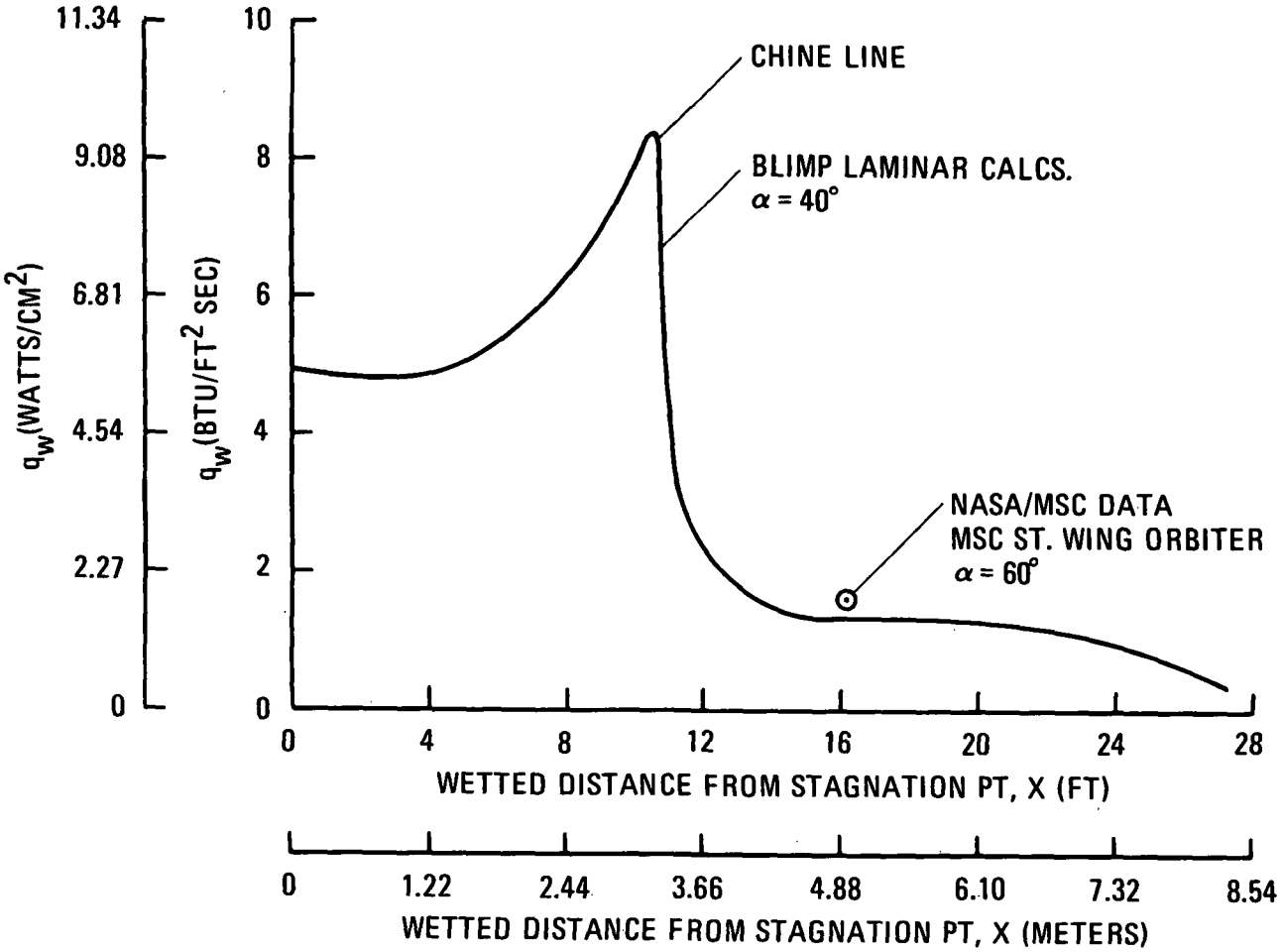


Figure 17

(Figure 18)

The results of the finite difference flow field for the 2-D cross section were used together with the TRW Shock Layer Analysis Program (Ref. 3) and the BLIMP Program to predict the location of the fuselage shock inpingement on the Orbiter wing. A simulated wing was attached to the chine line of the cross section at a dihedral angle of $7^{o}$. Four points inboard of the shock intersection point on the wing and one point outboard were used to make calculations. The flow field around 2-D airfoils at these points was calculated by the Shock Layer Program based on input from the finite difference 2-D analysis and neglecting the flow velocity in the spanwise direction of the wing. The resultant heating rates as computed by the BLIMP Program are seen in figure 18 compared with MSC arc jet data (C. Scott) at $60^{o}$ angle of attack. It may be seen that good agreement exists using either of two correlation expressions relating flat faced cylinder heating rates to hemisphere heating rates as reported by C. Scott. The location of the bow shock impingement on the wing appears to be between 35 and 40% of the exposed span as shown by both experimental data and theoretical analysis.

## COMPARISON OF PREDICTED HEATING RATES ON ORBITER WING LEADING EDGE AT 60° ANGLE OF ATTACK WITH MSC ARC JET TEST DATA

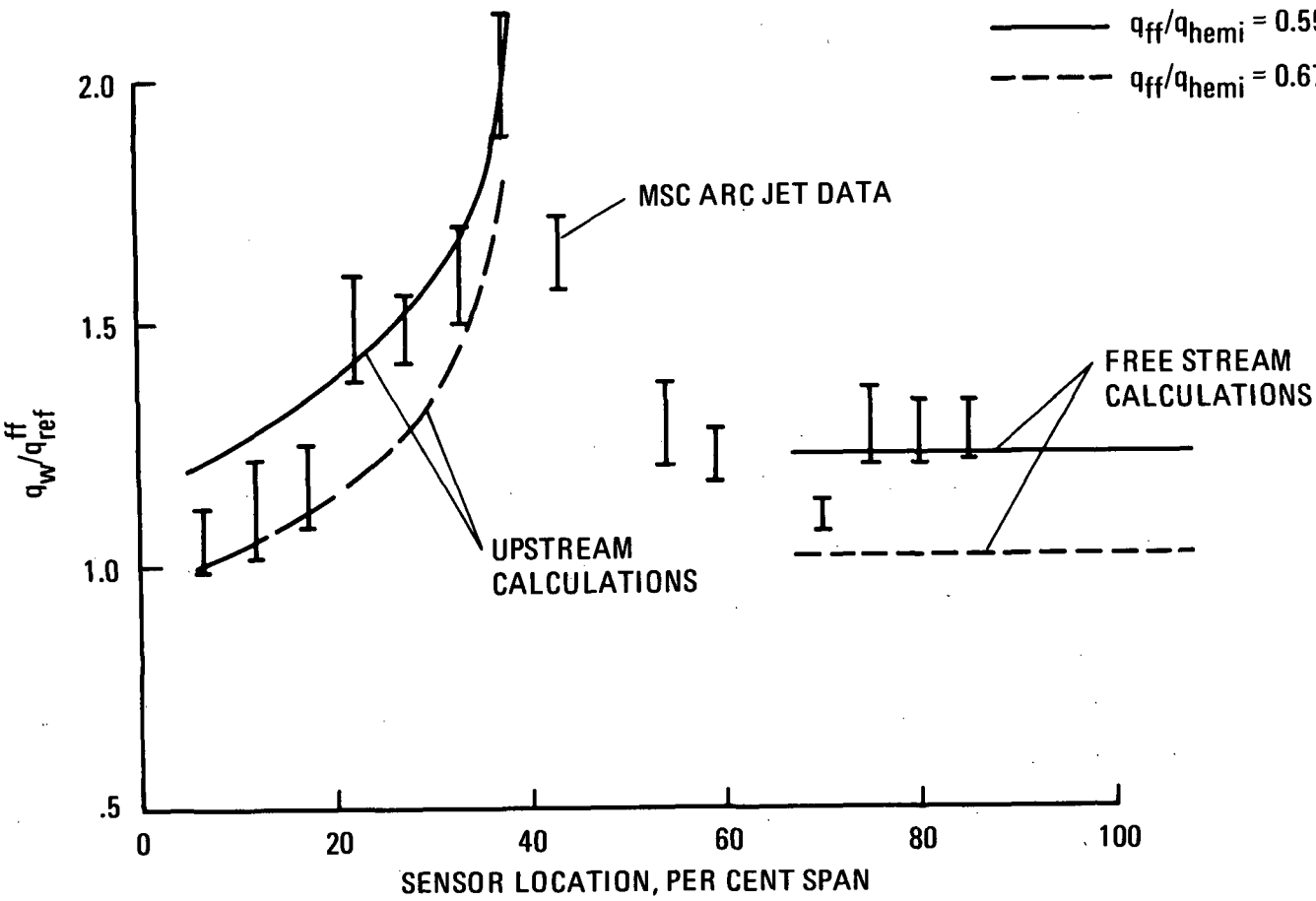


Figure 18

(Figure 19)

A similar procedure for an airfoil at $\alpha = 40^{o}$ was performed for the 3-D finite difference flow field by using the property values at cycle 1000 (just upstream of the wing leading edge) as input. In this analysis the velocities along the span as well as along the axis were allowed to vary. Also about 12 points along the span were considered. The predicted heating rates on the airfoil at $\alpha = 40^{o}$ which were obtained from BLIMP, based on pressure distributions from the Shock Layer Analysis Program, are shown in this figure. Notice that very good agreement resulted with Ames test data (Ref. 10) for an MSC straight wing Orbiter model at $\alpha = 40^{o}$ and that the shock impingement point was about 37-38% of the exposed span.

## HEATING RATES ON LEADING EDGE OF ORBITER WING AT 40°

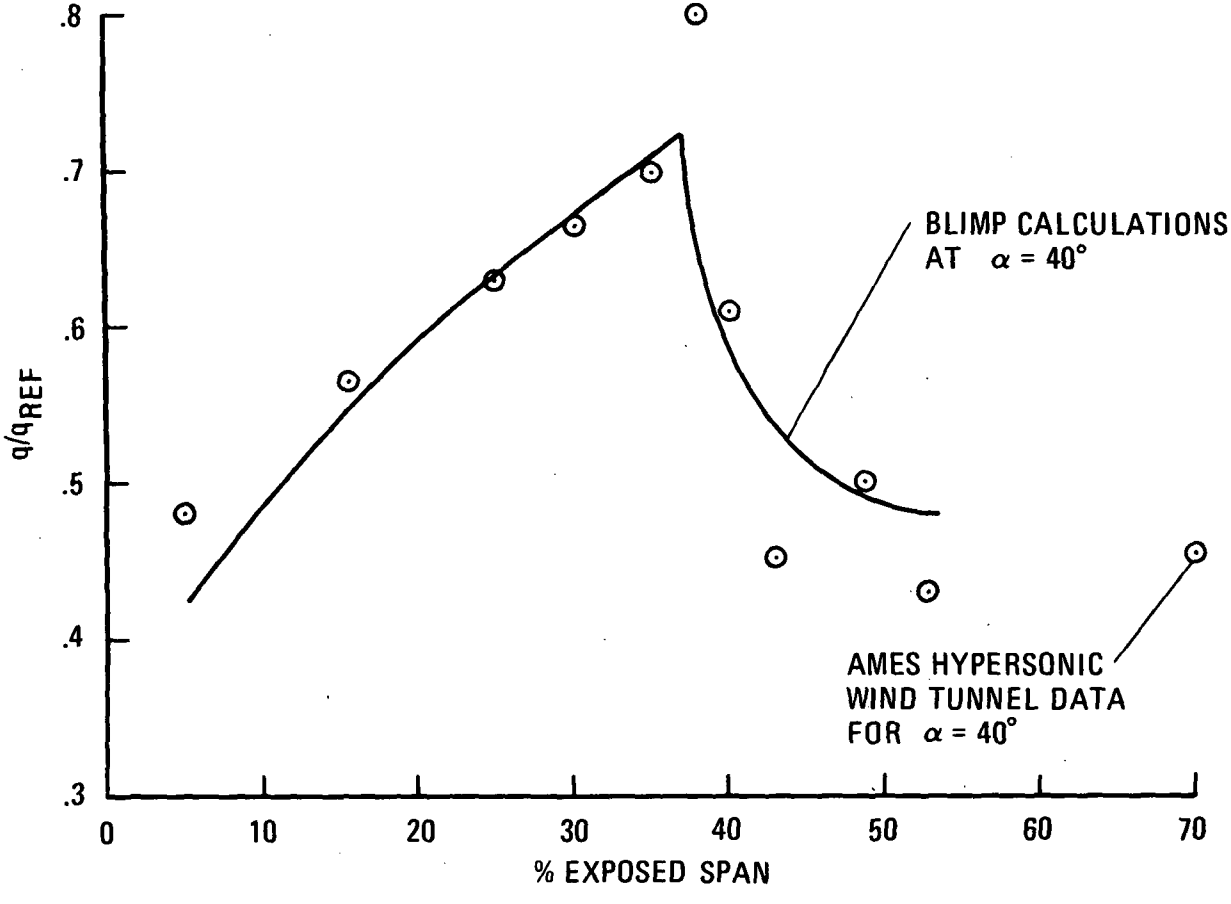


Figure 19

## CONCLUSIONS

This paper has presented a summary of a reentry flow field and heating analysis performed for the MSC straight wing Orbiter at high angle of attack. Rarefied flow fields and heating were calculated by the Monte Carlo Direct Simulation Technique at high altitudes. For lower altitudes a 2-D unsteady and 3-D steady finite difference method combined with an artificial viscosity technique was used. Flow fields and associated heating rates were computed for flat plates, Orbiter fuselage cross sections and airfoils, and 3-D representations of the Orbiter for a wide variety of free stream conditions, molecular models, $\alpha$, $\gamma$, surface reflection, etc.

It was felt that this study contributed to the state of the art in flow field computational techniques for both rarefied and continuum flows. The Monte Carlo technique provided a more accurate method for analyzing flows in the transition and merged layer regimes which previously had been treated by a combination of free-molecule and continuum theories. The finite difference methods were able to treat more accurately the continuum flows behind both detached and attached shock waves because of the modified artificial viscosity approach. The finite difference method together with the shock layer and heating analysis for airfoils was able to provide an accurate definition of the Orbiter bow shock/wing shock interaction region. In many cases where experimental data was available, good and in some cases excellent correlation was obtained between these flow field and heating methods and the experimental data, thus verifying that the data was adequate for Space Shuttle Orbiter preliminary design purposes.

## REFERENCES


1. Rochelle, W. C., Vogenitz, F. W. and D'Attorre, L., et. al., "Final Report - Space Shuttle Vehicle Reentry Flow Field Analysis", TRW Systems Rpt. No. 16209-H002-R0-00, 19 July 1971
2. Vogenitz, F. W. et. al., "Monte Carlo Direct Simulation Technique - User's Manual", TRW Systems Rpt. No. 16209-001-R0-00, 12 July 1971
3. Gomez, A. V., "Hypersonic-Blunt Body, Shock Layer Analysis Program (AH002A)," TRW Systems Rpt. 70.4352.30-02, 8 May 1970
4. Bartlett, E. P., and Kendall, R. M., "Non-Similar Solution of the Multicomponent Laminar Boundary Layer by an Integral Matrix Method", Aerotherm Corp. Rpt. 66-7, Part III, March 1967
5. Wilkinsen, H. R. and Heimler, G. H., "Aerodynamic Surface Heating Program - Program No. AH005H", TRW Systems Rpt. 3123.22-172, 9 Oct. 1967
6. Bartlett, E. P., et. al., "User's Manual - Boundary Layer Integral Matrix Procedure, Version C (BLIMPC), Aerotherm Rpt. No. UM-70-20, June 22, 1970
7. Vidal, R. J. and Bartz, J. A., "Experimental Studies of Low-Density Effects in Hypersonic Wedge Flows", Rarefied Gas Dynamics, Vol. I, 1965
8. Rochelle, W. C., "A Review of Hypersonic Rarefied Flow Over Sharp and Blunted Flat Plates at Angle-of-Attack", TRW Systems Rpt. No. 70.4352.16-2, 17 March 1970
9. Lee, D. B., "Aerothermodynamic Data on MSC Space Shuttle", NASA/MSC Memo ES5/7-10(0)/163(m), 14 July 1970

10. Marvin, J.G., et. al., "Flow Fields and Aerodynamic Heating of Space Shuttle Orbiter", Paper Presented at Space Shuttle Technology Conference, Langley Research Center, 24 March 1971.